

**Permian Secular Variation
of the Ayaguz formation in Kazakhstan**

by

ZACHARY M. MENZO

Submitted as an Honors Thesis.

Department of Earth and Environmental Sciences

The University of Michigan

April 2013

Accepted by



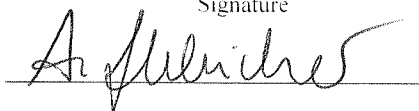
Signature

R. VAN DER VOO

Name

April 17, 2013

Date



Signature

Anja Schleicher

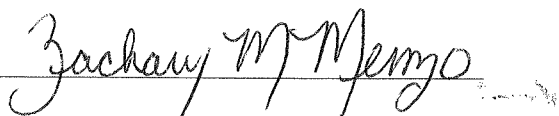
Name

April 17, 2013

Date

I hereby grant the University of Michigan, its heirs and assigns, the non-exclusive rights to reproduce and distribute single copies of my thesis, in whole or in part, in any format. I represent and warrant to the University of Michigan that the thesis is an original work, does not infringe or violate any rights of others, and that I make these grants as the sole owner of the rights to my thesis. I understand that I will not receive royalties for any reproduction of this thesis.

Permission granted



**Permian Secular Variation
of the Ayaguz formation in Kazakhstan**

by

ZACHARY M. MENZO

4/16/2013

Department of Earth and Environmental Sciences

The University of Michigan

March 2013

Abstract:

This study uses 60 individual volcanic flows from the Early Permian in eastern Kazakhstan with the intention of analyzing to what extent secular variation of the geomagnetic field may be reduced during the Kiaman (Permo-Carboniferous) Reversed Polarity Superchron (KRPS). Such a study can be important because the confirmation of a relationship between secular variation and polarity reversal frequency during the Permian would allow for the use of paleosecular variation (PSV) data to infer the dynamo stability in the past, something that is currently not possible for times earlier than 160 Ma. The samples analyzed for the study were collected from a thick pile in the Chingiz Range of NE Kazakhstan with a U/Pb age of 283 ± 2.4 Ma. The resulting data were compared to the data obtained by Dr. Bazhenov, who collected samples from the same volcanic pile for a parallel investigation. Nearly all of the paleomagnetic directions obtained in thermal demagnetization are seen to be SW and up, with a mean paleopole position at longitude (331.4E), and south-latitude (-37.9) confirming the expected mean Permian pole position. The resulting data also matched the anticipated high precision parameter (49.4), indicative of a stable geodynamo. This study therefore validates the correlation between secular variation and polarity reversal frequency.

1. Introduction:

Within the fluid outer core of the Earth, a self-excited dynamo occurs which ultimately generates the planet's magnetic field [Butler, 1992]. Over the course of

hundreds to thousands of years, this dynamo action produces internal variations in the geomagnetic field, referred to as secular variation [Biggin, 2008]. Recently, researchers, such as Biggin, have attempted

to correlate secular variation to the Earth's reversal frequency, based on the assumption that extreme events of dynamo action may well result in polarity reversals. These chance events are driven by an increased flow of liquid iron alloy, making up the geodynamo in the outer core [Biggin, 2012]. It has been suggested that in times of low reversal frequency (superchrons), the dipole nature of the Earth's geomagnetic field should be stable resulting in lower secular variation. If this is true, then PSV can be utilized to infer dynamo stability in the past.

The above controversial notion is currently being tested by a series of PSV analyses [Biggin, 2008]. In order to get first order descriptions of PSV, researchers including McFadden et al. [1991] and Tarduno et al. [2002], collected a series of lava flow samples. Sedimentary sections also yield paleomagnetic data [e.g. Tauxe and Hartl, 1997], however their slow depositional nature tends to average out

variations in the field, which can be challenging to quantify. Moreover, post-depositional processes such as compaction may distort the distribution (and hence, the SV parameters) of directions. Therefore, lava samples serve as more reliable data for statistical analyses of PSV relative to sedimentary rocks [Biggin, 2008]. The lava's data are then converted, using the dipole formula, into the virtual geomagnetic pole (VGP) [Butler, 1992]. The VGP's are considered "spot readings" of the total geomagnetic field.

Once a sampling interval long enough to allow for the proper averaging is completed, secular variation trends are then able to be observed on a VGP dispersion diagram or a VGP directional scatter diagram. VGP diagrams are a commonly used tool, which plots the angular dispersion or scatter relative to the (paleo)latitude (**Figure 1**). The directional scatter of a population of directions is calculated

through the precision parameter, k , with high precision parameter suggesting less scatter among the VGP positions. From these diagrams it can be observed that during times of high reversal frequency, there is a greater scatter of VGP positions (i.e. secular variation) at lower latitudes relative to times of low reversal frequency [Biggin, 2008].

However, one of the main limiting factors in most paleomagnetic studies is the lack of units suitable and abundant enough to analyze. In order to calculate the PSV, either from paleomagnetic directions, or from paleopoles, there is a minimum number of cooling units that is required before the data obtained can be considered reliable. With the number of large lava piles quickly diminishing with Phanerozoic age, there are few or no data to analyze before 160 Ma [Heunemann *et al.*, 2004].

Fortunately, previous research on large lava sequences of Paleozoic age in

Kazakhstan and Kyrgyzstan has documented suitable primary Paleozoic magnetizations that can be used to determine new PSV data for Permian and Devonian times. Comparisons will hopefully reveal correlations between SV trends and the very low polarity reversal frequency in the Permian, giving insight into the long term evolution of the magnetic field. The Devonian results have been published [Bazhenov *et al.*, 2013] and the Permian is reported here.

The purpose of this paper is to analyze the remanence of the 282 individual samples obtained from Early Permian lavas in eastern Kazakhstan. The later Permian marks a transitional time from the KRPS, (Pennsylvanian- Early Permian), to a Late Permian time of high reversal frequency which continued into the Triassic. Therefore, the results expected from the Early Permian should reveal low secular variation, whereas latest Permian results

(e.g., from the Siberian traps) are to be compared eventually (once properly analyzed) in order to detect a correlation between frequent polarities and large PSV.

2. Geological Setting:

Kazakhstan, is a country primarily located in Central Asia (**Figure 2a**) in the Ural-Mongol fold belt (**Figure 2b**). Its evolution began during the Late Precambrian, but peaking first in the Late Ordovician- Early Silurian, when many tectonic units began to amalgamate into microcontinents built upon Proterozoic basement [Alexeiev *et al.*, 2008]. This proceeded until the Early- Middle Devonian, when subduction driven volcanism began the 150 million year long migration inward, inducing both stratigraphic and angular unconformities on the now active continental margin and ending in the Late Permian [Levashova *et al.*, 2003]. While the sedimentation continued to occur, Kazakhstan collided with Siberia (in the

northeast), Baltica (in the northwest) and Tarim (in the south) inducing a clock-wise, rotation on eastern Kazakhstan [Abrajevitch *et al.*, 2008].

Throughout the Carboniferous and Early Permian, volcanic layers continued to be deposited as the orocline was undergoing bending [Levashova *et al.*, 2003, Van der Voo *et al.*, 2006]. Finally, in the Late Permian, the last volcanic layers were deposited. For the remainder of the Permian, some portions of the orocline continued to rotate, resulting in its present position (**Figure 3**). This indicates that the Ural Ocean, between Siberia, Baltica and Kazakhstan tectonic elements, was not a large and multi-plate system during mid to late Paleozoic times [Levashova *et al.*, 2007].

The samples analyzed for the study were collected from a thick pile of flows in the Chingiz Range of NE Kazakhstan (**Figure 4**). The localities of the sites were

on the limb of a wide and gentle north-south trending syncline [Levashova et al., 2003]. The age determination of the volcanic [J.G. Meert, pers.comm. 2012] yielded 283 ± 2.4 Ma. (i.e. in the middle of the Early Permian). The Early Permian samples were collected from a series of 5 to 15m-thick flows. The more resistant flows created a series of parallel ridges 50m high and 10km long. There were no faults or small-scale (fault-conjugated) folds observed [Sal'menova and Koshkin, 1990].

3. Methods:

For the purposes of this study, 282 individual samples were collected from 60 sites, each representing a lava flow, in eastern Kazakhstan, near Ayaguz during July, 2011. A parallel sampling effort was undertaken by Dr. Mikhail L. Bazhenov, who collected hand samples, later sawed into small cubes. For the Michigan team's collecting, the initial idea was to collect six to eight samples per site using a portable

Pomeroy drill. Cores were long enough to get 2 to 3 specimens per core. This was done for the first twenty sites. However, while collecting the final sample in the twenty-first site, the drill became non-functional and for each of the remaining sites, only four fist-sized samples were collected.

The azimuth and plunge were measured for a reference line on each core sample, using either a solar or Brunton compass and an inclinometer. Additionally, the strike and dip of bedding were determined with the use of a compass. Azimuth was marked on each core sample with the arrow pointing in the down direction. The orienting convention measured the plunge at 90° when the core orientation was horizontal. Conversely, a plunge of 0° meant that the core was vertical.

The hand samples were shipped to the paleomagnetic laboratory at the

University of Michigan. Once in the laboratory the samples were each leveled in a plaster-paris cast and left to dry. After the samples were properly solidified, they were drilled using a diamond-tipped drill press. On average, each sample yielded two cylindrical specimen, about 2.5 cm in diameter. Each sample was then dried, cleaned, cut into 2cm-height specimens, and finally, labeled with a non magnetic, temperature resistant paint [Dominguez, 2012]. Each sample was labeled utilizing a convention where each sample was given a number (AR 1- AR 282) and each specimen was denoted with an A,B and C if necessary. Also, if any samples were damaged during the trip or in the drilling process, they were then cemented back together using an alumina cement.

After the specimens were clean and labeled, they were brought to the Paleomagnetism, Structure and Tectonics Laboratory (PaSTeL) at the University of

Michigan. The laboratory equipment is stationed within a magnetically shielded room to prevent the acquisition of a viscous magnetization. Within the shielded room, the specimens were each thermally treated by an ASC TD-48 demagnetizer, resulting in a series of heating steps and sample re-measurements that isolates a characteristic natural remnance magnetization (NRM) [Dominguez, 2012]. The results were then plotted on a steronet projection as well as graphed on a Zijderveld plot.

The data were then compiled into a table and the values were inspected and compared to the data obtained by Dr. Bazhenov (MO-data). The Michigan (MI) bedding data, appeared to be somewhat more scattered, relative to the MO-data, but they have very similar overall mean bedding normals. The variation difference is attributed to the fact that the MI-data were single measurements at a given locality, whereas the MO-data are mostly

regional averages of multiple measurements, resulting in a lesser scatter. In **Figure 5** the normals to bedding are displayed on a common stereonet projection. Both the MO and MI-site mean data, yield a similar overall mean. It therefore can be justified to use a combination of the MI and the MO values as averaged bedding data (**Table 1, Table 2**). A site must yield at least three usable sample directions in order to calculate a reliable site mean or VGP position.

4. Directional Analysis:

During the course of the thermal demagnetization of a sample, the changing magnetization can be projected onto two orthogonal planes. Such a plot is called a Zijderveld diagram and displays both magnetization direction and intensity in a manner that makes it immediately clear whether multiple components of magnetization were superposed. The diagram will reveal linear segments

corresponding to the declination and inclination of a given isolated or removed component [*Dunlop, 1979*]. Approximately half the MI- samples presented well-defined first and second components of magnetization, which were removed sequentially in thermal treatment. At higher temperatures, the samples showed a clean univectorial decay to the origin, indicating the sample's remanence has been fully characterized, as seen in **Figure 6**. The directions of about half of the samples remained highly clustered until higher thermal treatments were applied, at which time the sample remanence decayed to the origin (**Figure 7**). Most samples presented at least one step in between the clustering and the origin. The few samples that did not produce a Zijderveld diagram similar to the ones previously mentioned, indicating either a single component of magnetization (**Figure 8a**) or three components of magnetization (**Figure 8b**) with a clean

decay to the origin. Most samples produced clean decay diagrams, while other samples, while indicating some noise (**Figure 8c**), were still able to be used. Only a handful of samples were considered too "noisy" for further study. (**Figure 8d**)

A comparable view of the data can be seen in terms of the site mean data, which are presented in terms of declination and inclination. **Figure 9** shows the Michigan analyzed, tilt- corrected, data with a mean site declination and inclination of (252.2, -54.5). Site- mean ChRM directions yielded 47 reliable site mean data, resulting in an adequate sampling of secular variation. Sites were deemed not reliable if the radius of the cone of 95% probability (i.e. $\alpha_{95} \geq 15$ dg, which is dependent on the number of samples used) was exceeded, or if the precision parameter condition (i.e. $k \geq 15$) was not met. Further analysis, showing the site mean density distribution can be seen in **Figure 10**.

Finally, one of the main ways to present PSV data is to analyze the VGP directional scatter relative to (paleo)latitude. To obtain scatter data, a pole position (VGP) is calculated from each site's characteristic component remnance magnetization (ChRM). Then these VGP's are averaged, yielding a mean paleopole position (latitude, longitude) as well as statistical parameters (e.g. K, A95.) Useable VGP site means have been projected onto a common steronet in **Figure 11**. From the reliable VGP positions a mean at an average longitude (331.4), and latitude (-37.9) was calculated, confirming the expected mean Permian pole position.

5. Discussion:

The main purpose of this study is to analyze the relationship between the Earth's polarity reversal frequency with the coeval secular variation. Since the mean paleopole calculated from the MI-data is consistent with the paleopole mean extrapolated from paleomagnetic data found ten years ago by

Levashova et al., [2003] (**Figure 12**) the MI-paleopole location of (331.4,-37.9) can be used, therefore validating the MI mean VGP position obtained. This is done by analyzing the VGP directional scatter against paleolatititude which is determined by a statistic that can provide a measure of the scatter of the population of directions. For this study the precession parameter, K , was used. The secular variation for this study shows a relatively large precision parameter and subsequent small scatter of the magnetic poles which is consistent with the expected results from the Early Permian. The mean precision parameter, K , for the 39.9° latitude is 49.4, which is corresponding to other precision parameters in the VGP directional scatter diagram during times of low polarity reversal frequency (**Figure 13**).

The low secular variation, or scatter, observed during the Permian, in eastern Kazakhstan can be attributed to the decreased heat flow through the Core-

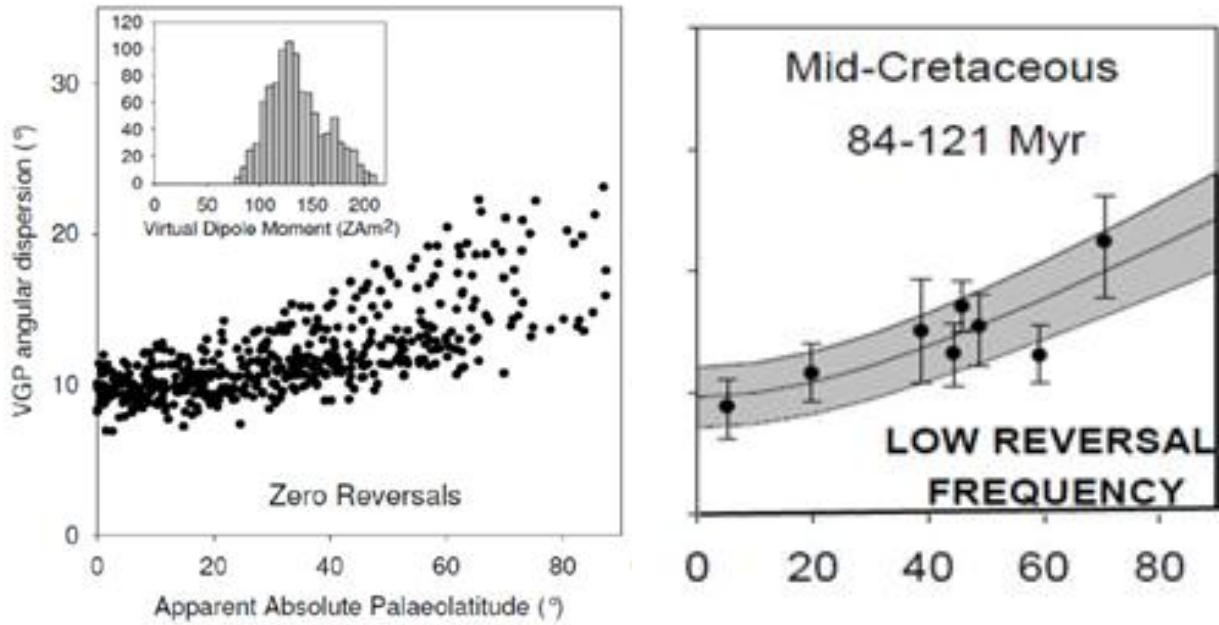
Mantle Boundary (CMB) leading to a greater geodynamo stability and consequently lower polarity reversals. During these superchrons, the dipole nature of Earth's geomagnetic field is increased (including the increase in geomagnetic field strength) and introducing less scatter in the VGP distribution. Consequently, secular variation and geodynamo stability are inversely correlated. Additionally this study indicates that the scatter vs. polarity reversal frequency relationship may also be applicable to older geological periods.

6. Implications:

In this study, 282 samples were collected from 60 sites within eastern Kazakhstan. The samples yielded site means and VGP locations which were used to determine an overall mean and statistical parameters pertaining to secular variation. The resulting data matched the expected VGP location with low scatter, indicative of a stable geodynamo. It can also be stated,

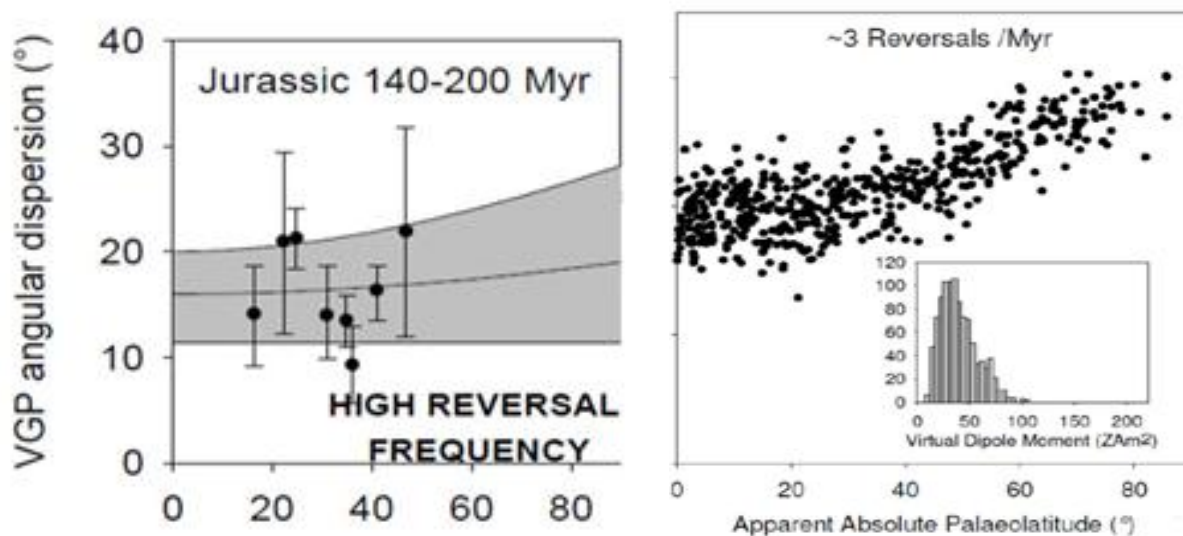
that the secular variation resulting from the MI-data fits the expected low directional scatter of the 39.9° latitudes. This I have attributed to the fact that lower latitudes are subjected to a greater influence of the stable, dipole magnetic field produced during the superchron. The stronger the dipole nature of the regional field, the smaller the resulting scatter among the VGP positions. In addition to giving a glimpse into the interaction between the Earth's outer core and mantle and overall geodynamo [Dominguez, 2012], this study is important because the confirmation of secular variation's relationship with polarity reversal frequency during the Permian, allows for the use of PSV data to infer the dynamo stability in the past.

7. Images:



(a)

Figure 1: VGP dispersion diagrams used to analyze secular variation. Plots VGP dispersion against paleolatitude (a) in time of low polarity reversal (e.g. Mid-Cretaceous), (b) in times of high polarity reversal (e.g. Jurassic) [Biggin, 2008].

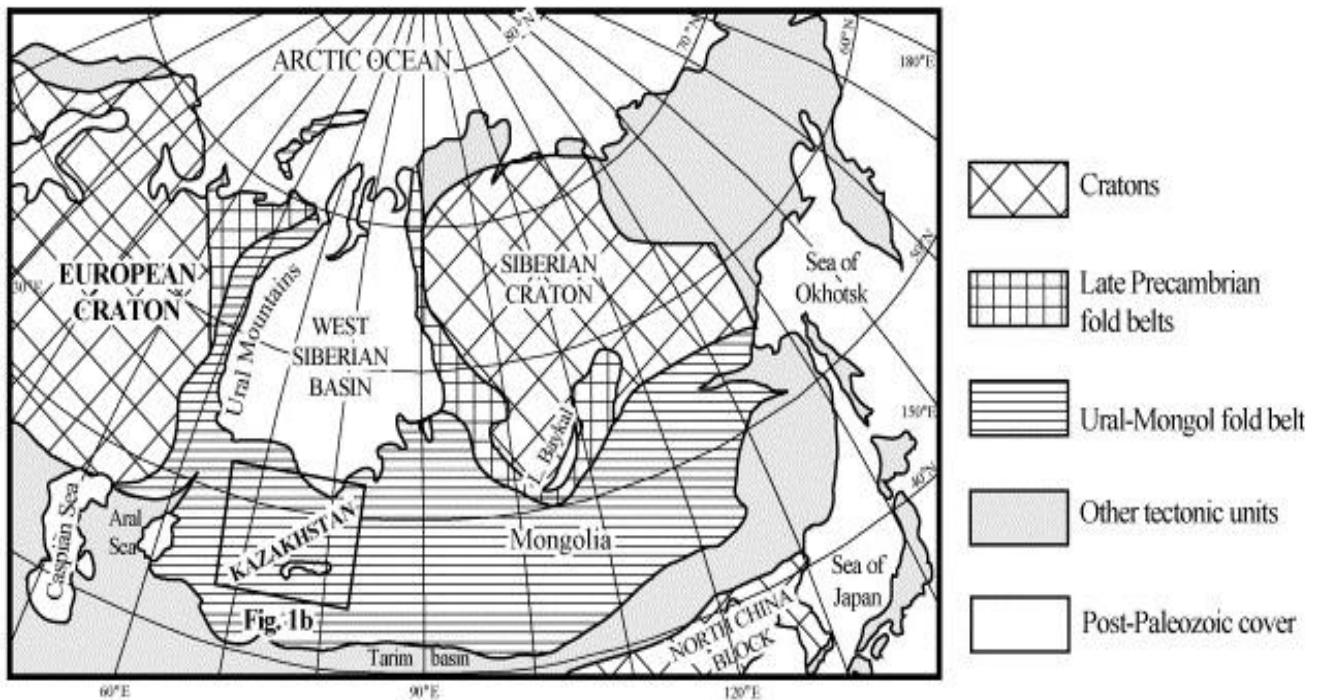


(b)



(a)

Figure 2: (a) Shows a map of Kazakhstan located in Central Asia. It is surrounded by Russia, China, Kyrgyzstan, Uzbekistan, and Turkmenistan, and also borders on a large part of the Caspian Sea. (b) Kazakhstan is an amalgamated microcontinents located in the Ural-Mongol fold belt [Levashova *et al.*, 2003].



(b)

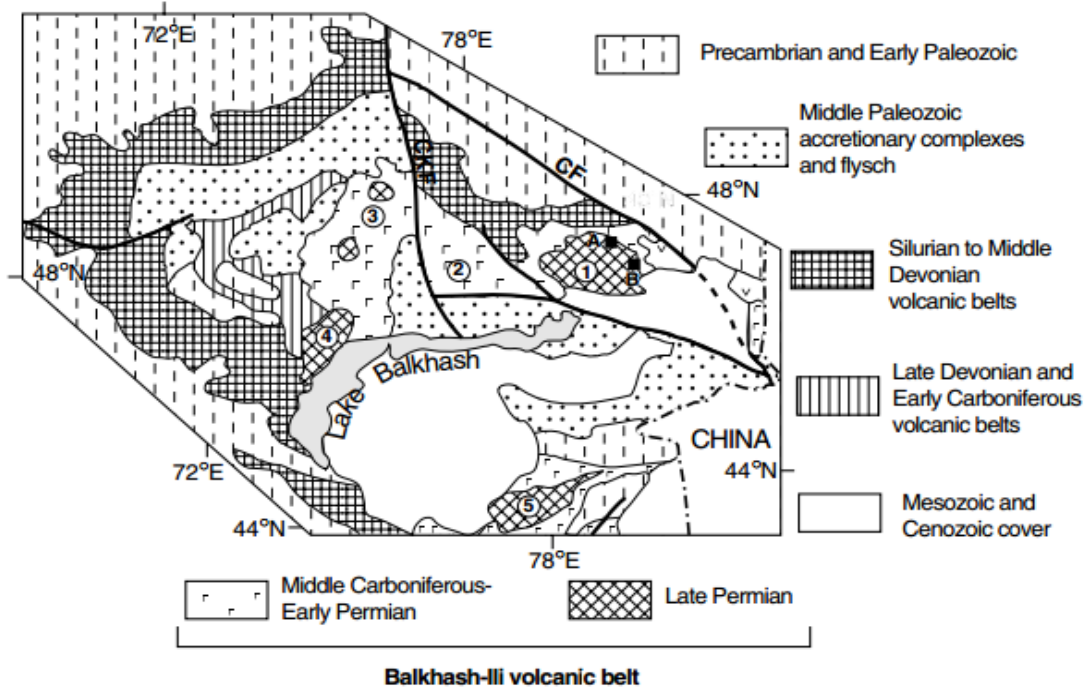


Figure 3: Gives the various distribution of volcanic flows of varying ages in East Kazakhstan [Levashova et al., 2003].

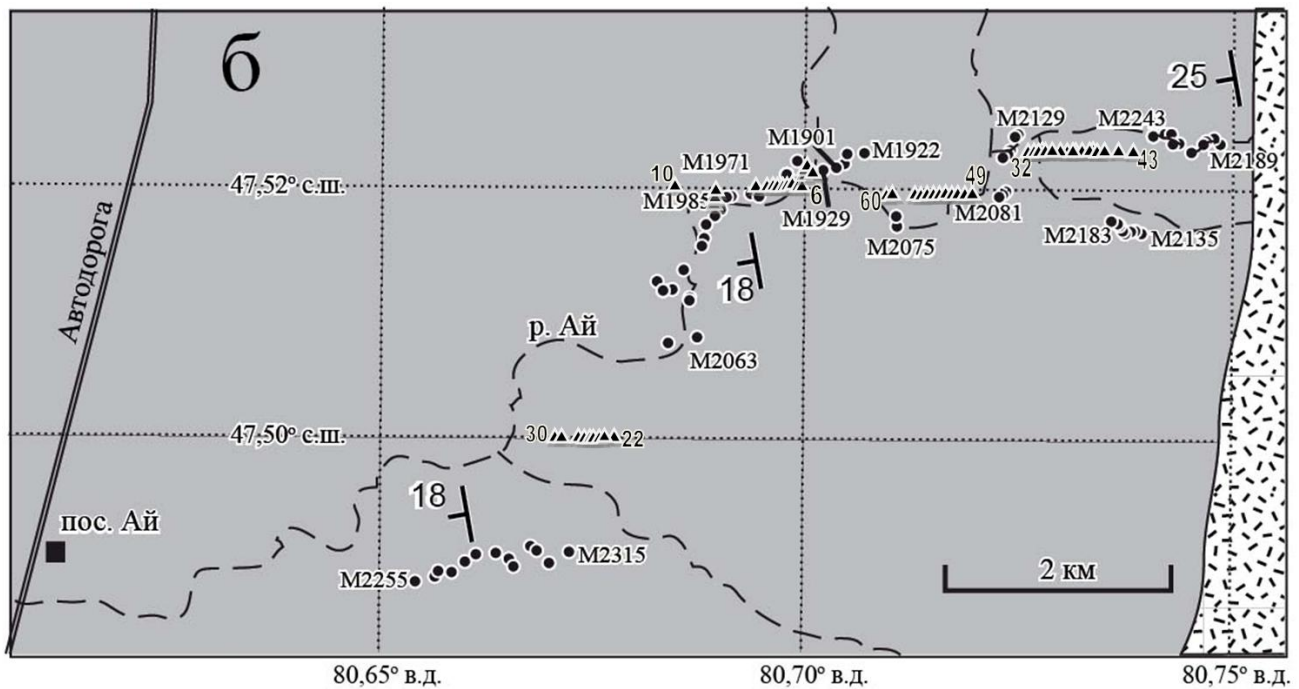


Figure 4: Location map of the various sites of which samples were collected. The circles represent sites sampled for the MO-data and the triangles indicates sites sampled for MI-data.

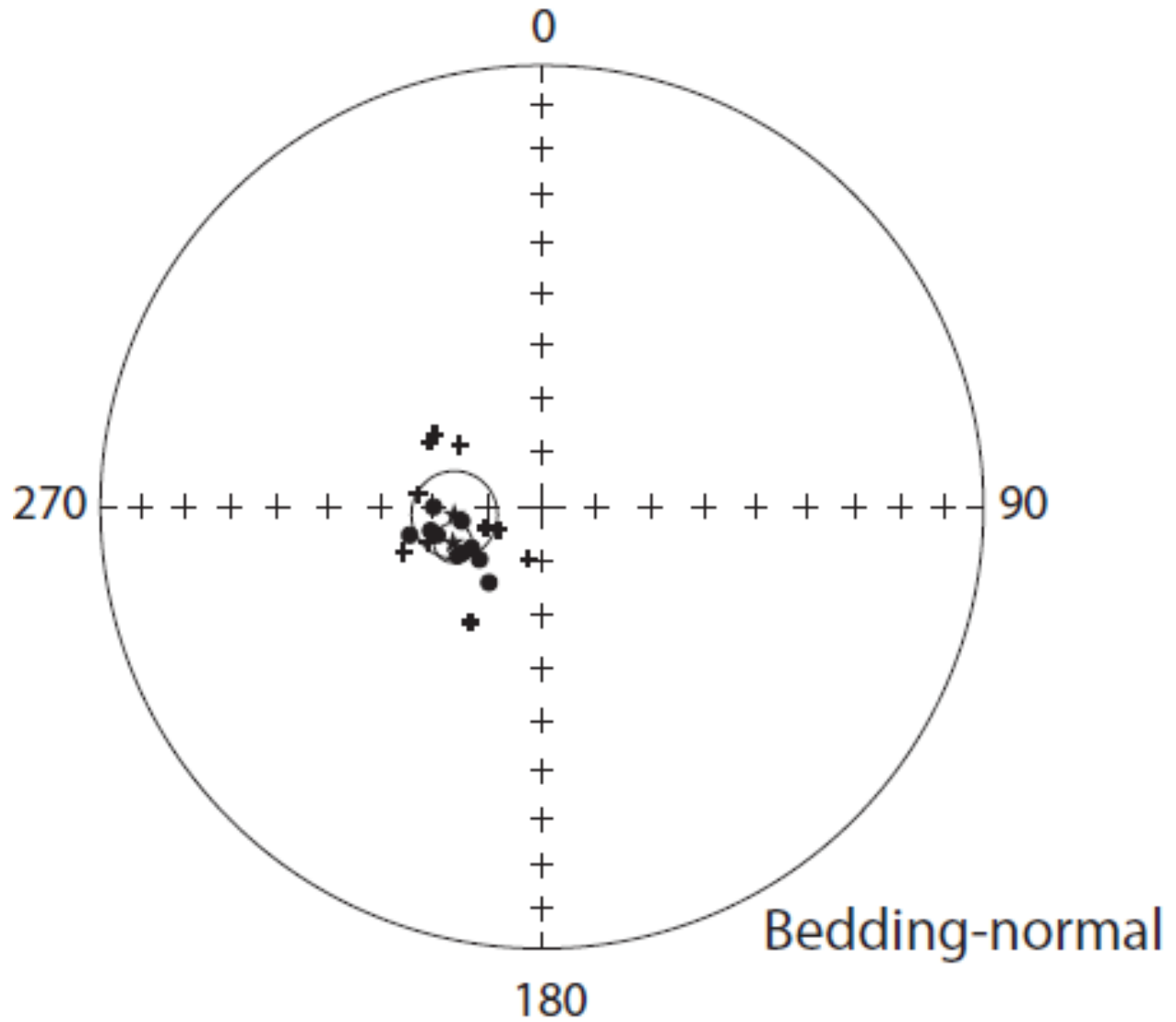


Figure 5: Orthographic projection of the bedding to normal data collected from both the MO-collection (circle) and the MI-collection (cross). The variation difference attributed to the fact that the MI-data were single measurements at a given locality, whereas the MO-data are mostly regional averages of multiple measurements, resulting in a lesser scatter.

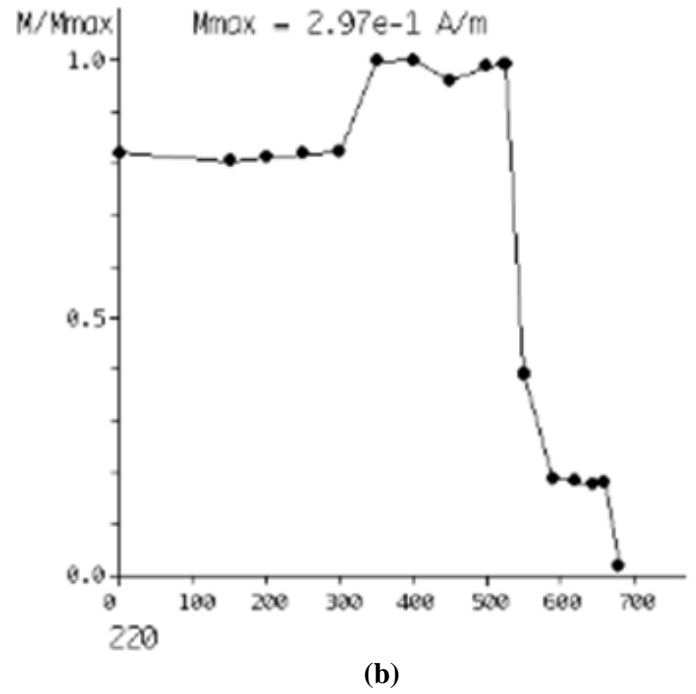
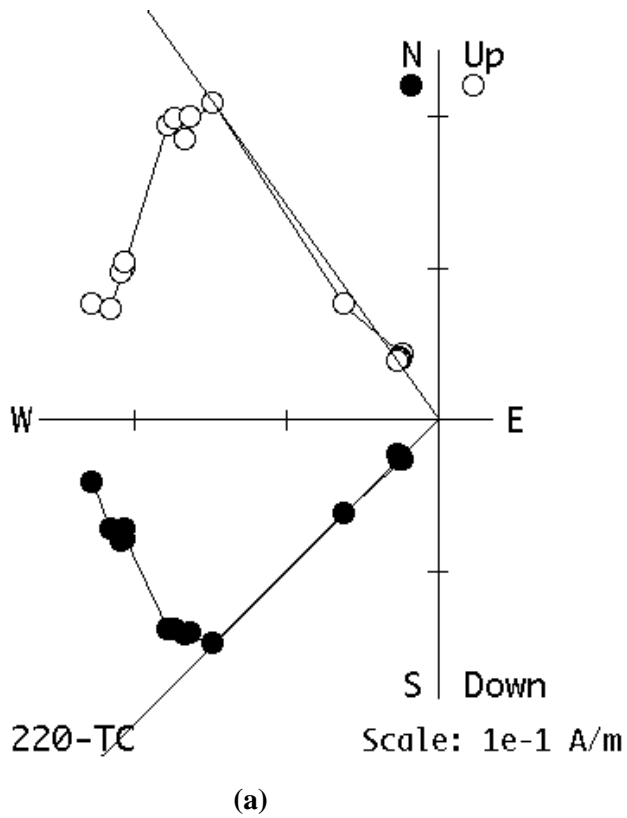
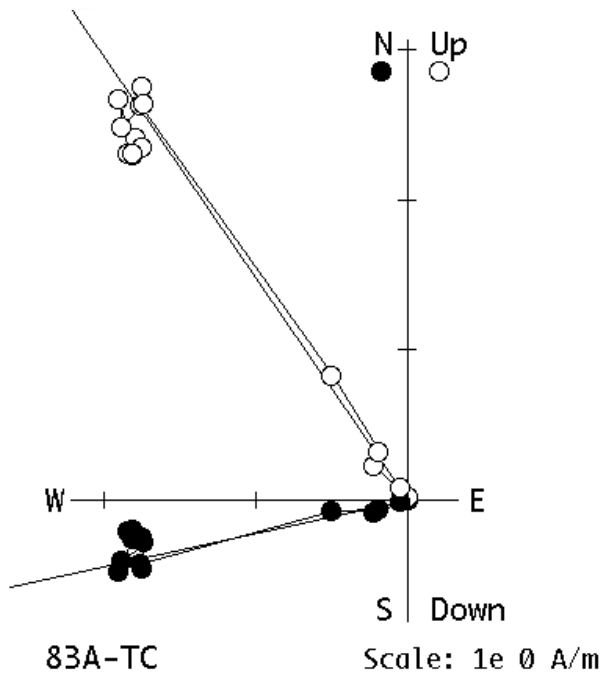
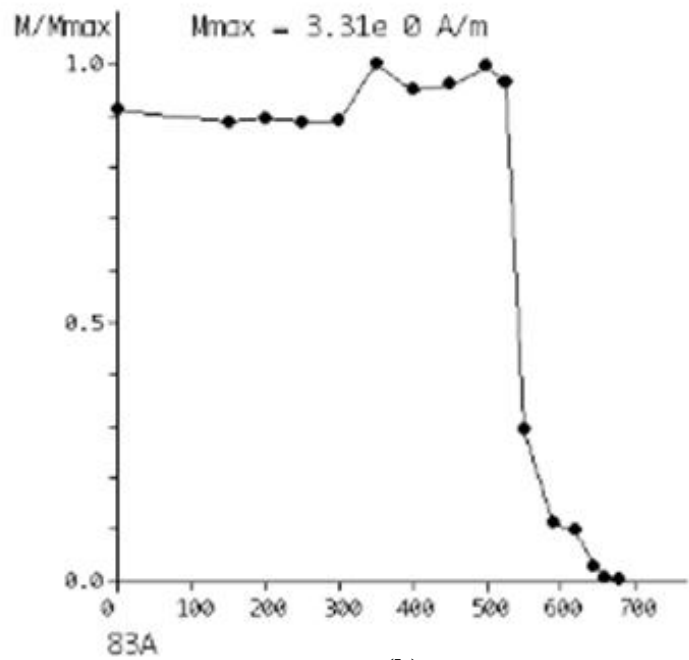


Figure 6: Demagnetization information for sample 220, showing its (a) Zijderveld diagram, indicating an overall southwest and up direction, and its (b) intensity diagram, indicating the presence of both magnetite and hematite. Sample 220 presented a well-defined first component of magnetization, which was removed with higher thermal treatment. Afterwards, the samples showed a clean decay to the origin



(a)



(b)

Figure 7: Demagnetization information for sample 83, showing its (a) Zijderveld diagram, indicating an overall southwest and up direction, and its (b) intensity diagram, indicating the presence of hematite. Sample 83 remained highly clustered until higher thermal treatments were applied, at which time the sample remnance decayed to the origin

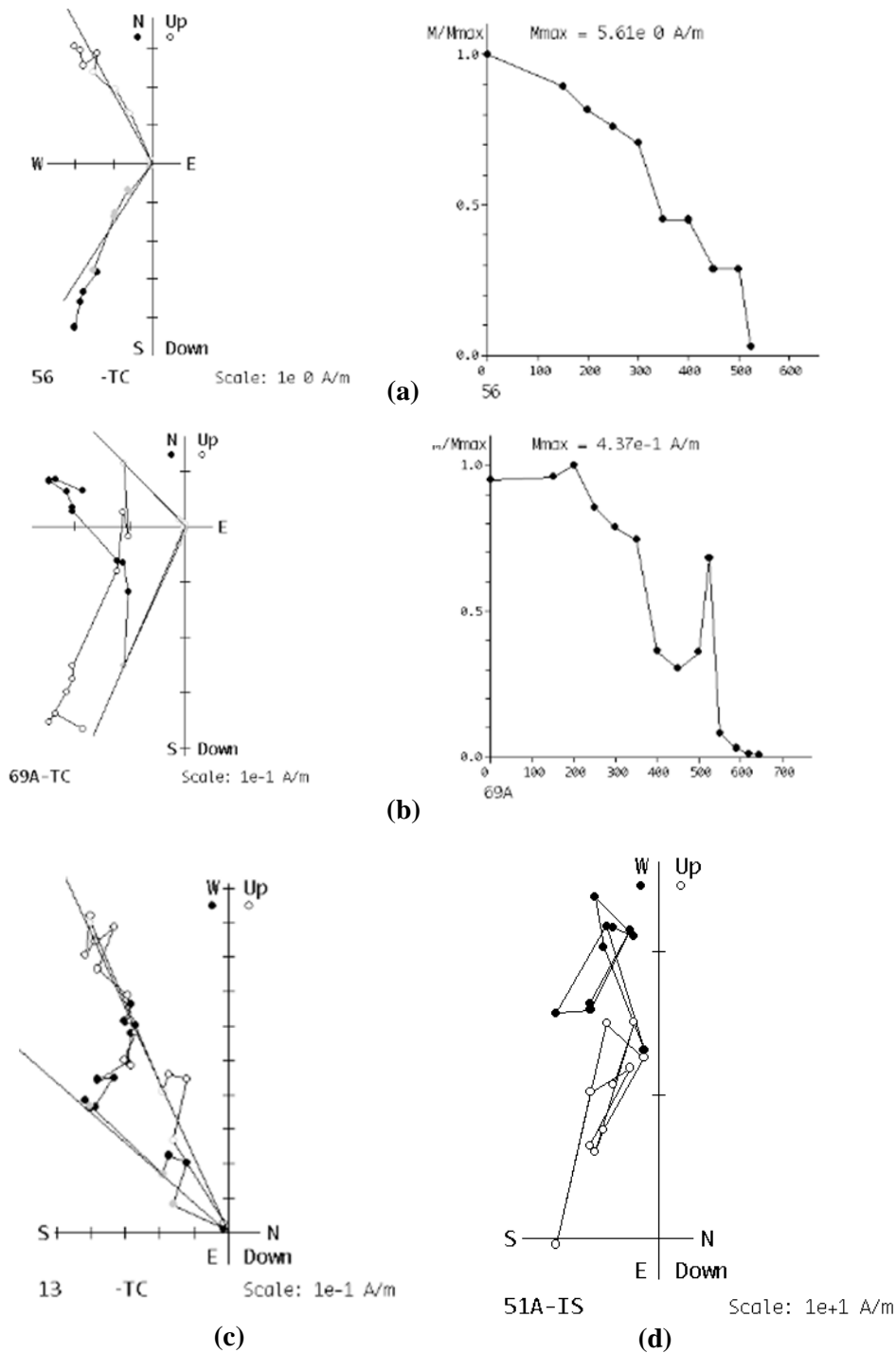


Figure 8: (a) Demagnetization information for sample 56, showing its Zijderveld diagram, indicating a single component of magnetization, and its intensity diagram.(b) Demagnetization information for sample 69, showing its Zijderveld diagram, indicating three components of magnetization, and its intensity diagram.(c) Demagnetization information for sample 13, showing its Zijderveld diagram, giving an example of a sample which produced noise but was still used. (d) Demagnetization information for sample 51, showing its Zijderveld diagram, giving an example of a sample which produced noise and was discarded.

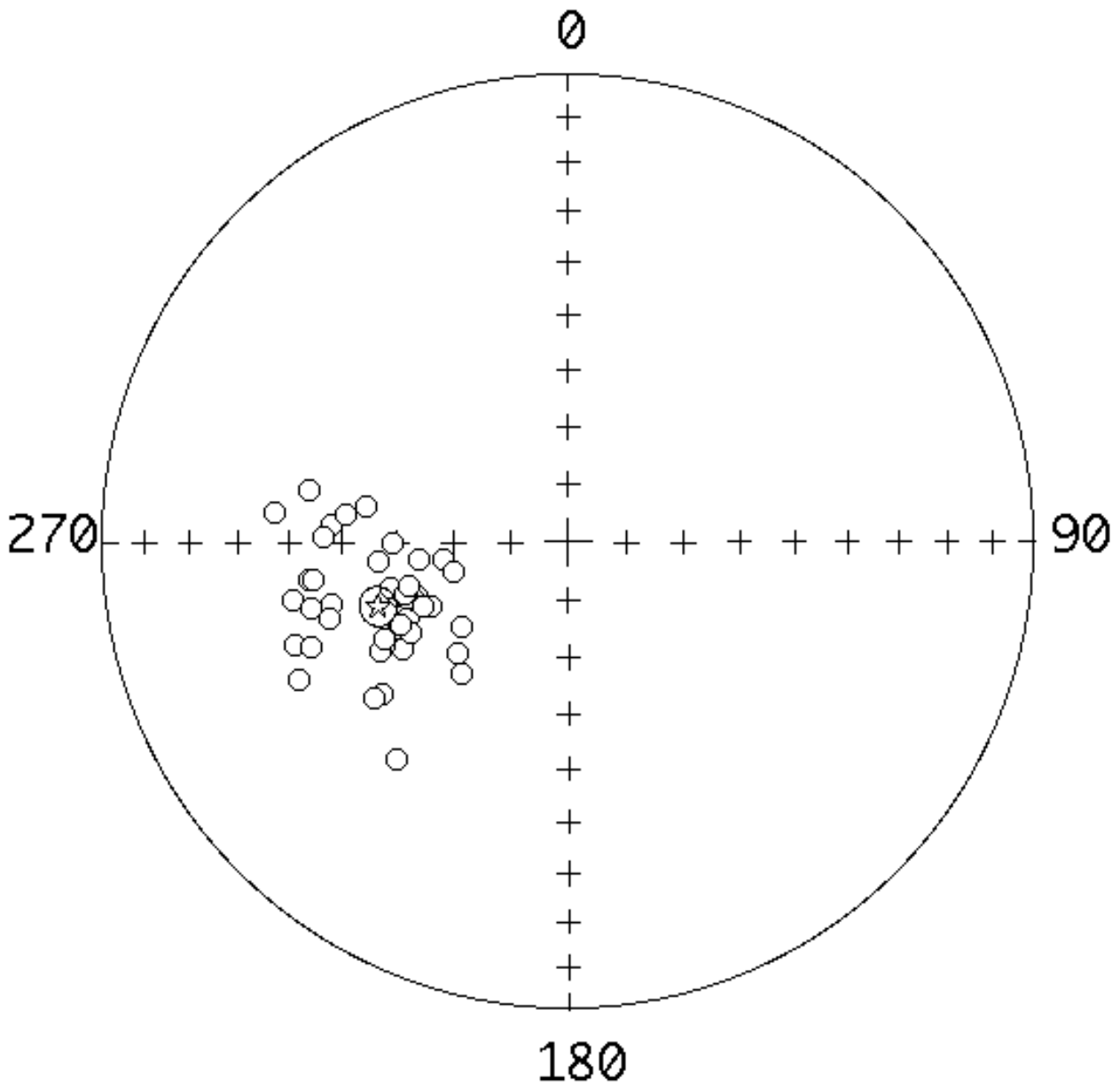


Figure 9: Orthographic projection of the Michigan analyzed, tilt- corrected, data with a mean site indicated by a star within a circle (Dg: 252.7, Ig:-54.5, **k: 43.1**, a95: 3.3).

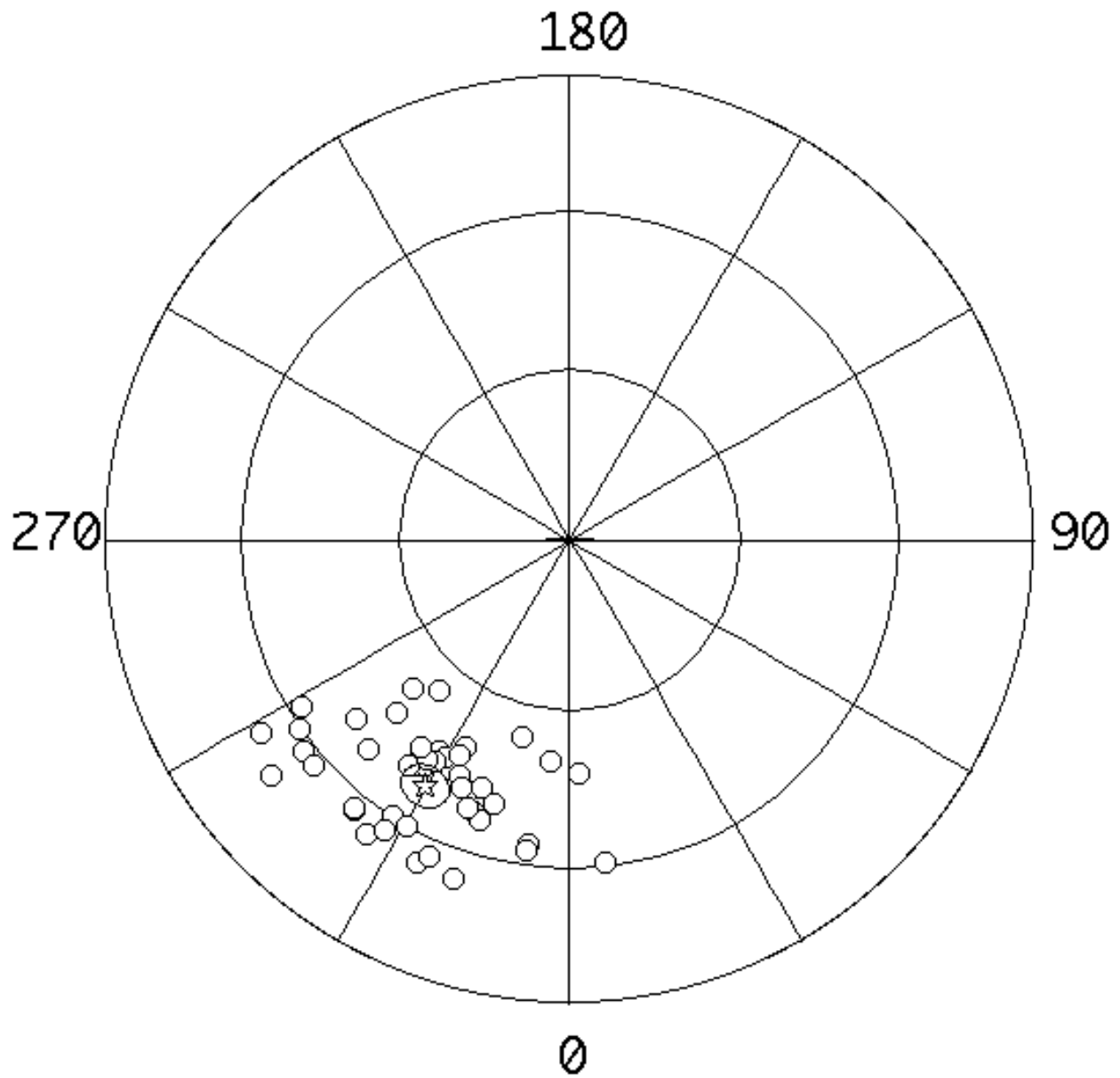


Figure 11: Orthographic projection of the various VGP locations. The total mean VGP location is indicated by a star within a circle (Long: 331.4 , Lat.: -37.9, **K: 49.4**, A95: 3.1).

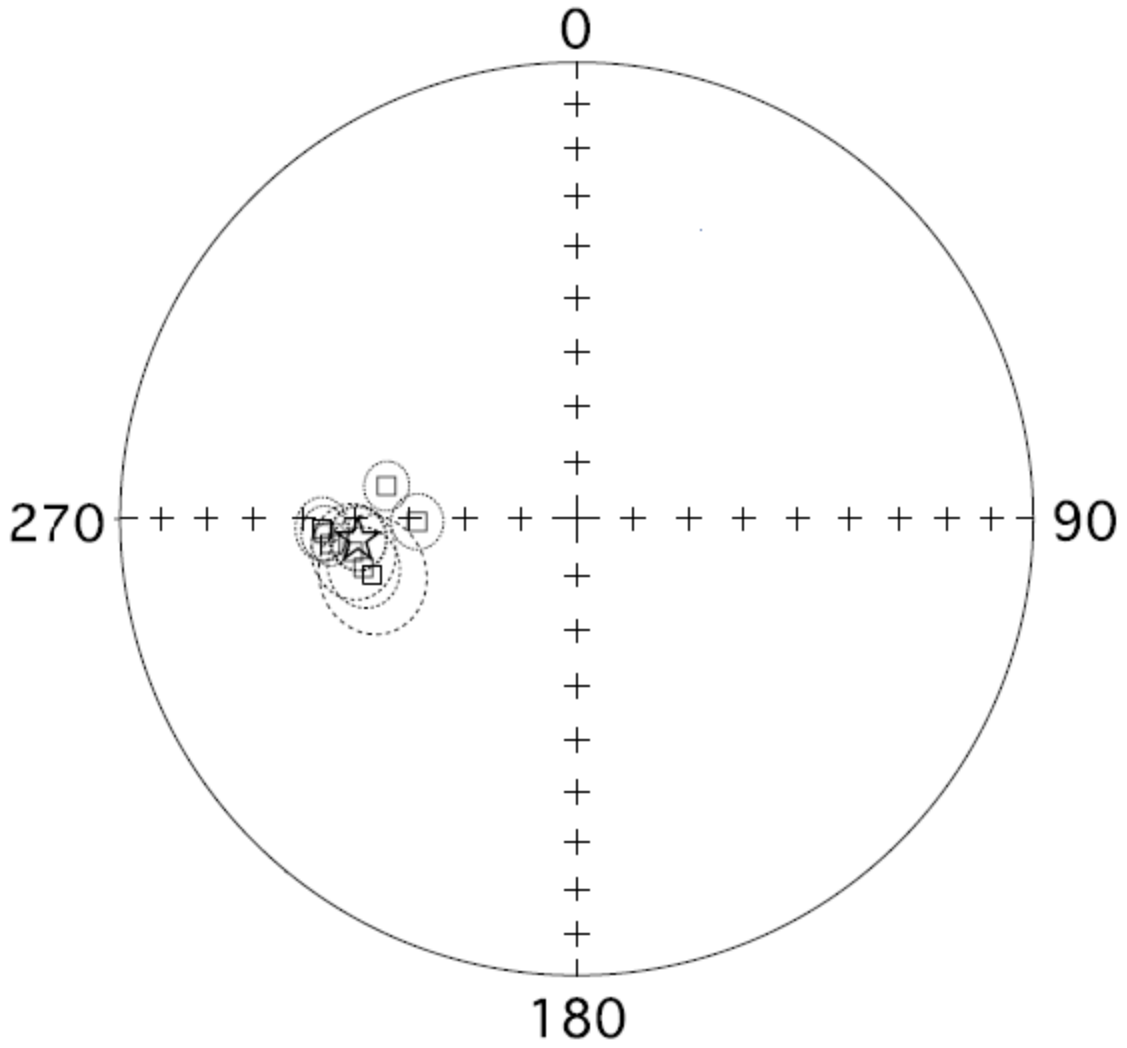


Figure 12: Orthographic projection of site mean from paleomagnetic data found ten years ago by *Levashova et al.*, [2003] with a mean site indicated by a star within a circle (Dg: 264.9 , Inc.: -50.2, K: 107, A95: 4.8, N: 8).

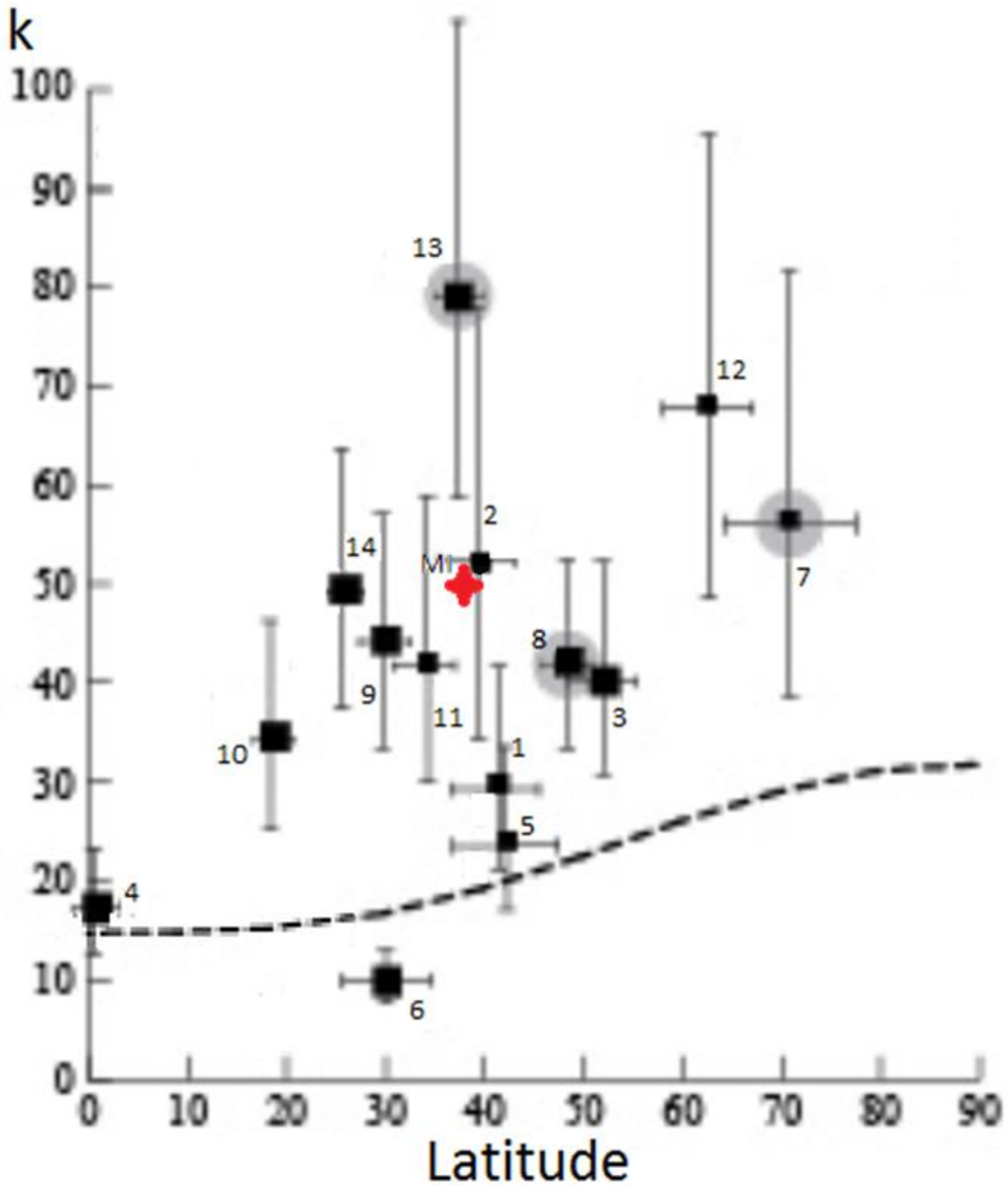


Figure 13: Calculated VGP directional scatter with the use of the precision parameter, as a function of latitude. The solid, black boxes represent the dispersion calculated from MO-data. The solid, red cross (marked MI) is the scatter of (49.4) calculated for the latitude of -37.9° [Bazhenov, pers.comm. 2012]. The dashed, black line indicates the projected VGP directional scatter according to the TK03GAD model [e.g. Tauxe and Kent, 2004].

8. Tables: General site information, organized by site number, with mean directions, statistical parameters, and VGP directions (*N1*: total number of samples collected; *N2*: number of treated samples).

Table 1: Site information yielded from in-situ site data.

<u>Site</u>	<u>Sample Range</u>	<u>N1</u>	<u>N2</u>	<u>GPS Long.</u>	<u>GPS Lat.</u>	<u>Dg</u>	<u>lg</u>	<u>VGP Long.</u>	<u>VGP Lat.</u>	<u>k</u>	<u>Q₉₅</u>
1	1-6	5	6	E 80° 42.205	N 47° 31.27	268.3	-30.1	315.7	-16.4	22.1	16.6
2	7-12	4	6	E 80° 42.140	N 47° 31.27	235.8	-41.6	347.7	-29.1	23.4	16.2
3	13-18	6	6	E 80° 42.138	N 47° 31.36	234.7	-29.7	349.6	-21.4	44.2	10.2
4	19-24	6	6	E 80° 42.147	N 47° 31.47	241.4	-37.3	342.4	-25.3	125.7	6.0
5	25-30	6	6	E 80° 42.139	N 47° 31.57	256.1	-27.9	329.6	-17.3	16.3	19.6
6	31-36	6	6	E 80° 42.155	N 47° 31.59	254.6	-41.9	329.0	-26.7	64.3	8.4
7	37-42	5	6	E 80° 41.890	N 47° 31.19	247.7	-45.2	334.8	-30.2	73.7	9.0
8	43-48	4	6	E 80° 41.877	N 47° 31.15	251.9	-44	331.2	-28.3	18.4	18.3
9	49-54	5	6	E 80° 41.871	N 47° 31.17	276	-26	309.2	-12.7	37.1	12.7
10	55-60	3	6	E 80° 41.86	N 47° 31.19	230.1	-42.6	353.2	-31.6	40.4	19.6
11	61-66	5	6	E 80° 41.871	N 47° 31.23	244.4	-43.0	332.6	-27.9	26.6	15.1
12	67-72	5	6	E 80° 41.652	N 47° 31.15	224.8	-24.2	1.0	-19.7	25.2	15.5
13	73-78	4	6	E 80° 41.826	N 47° 31.14	253.4	-39.7	329.8	-25.3	23.2	14.2
14	79-84	5	6	E 80° 41.749	N 47° 31.15	252.6	-40.3	330.9	-25.7	78.4	8.7
15	85-90	6	6	E 80° 41.781	N 47° 31.16	251.5	-42.1	331.8	-27.0	42.6	10.4
16	91-96	6	6	E 80° 41.814	N 47° 31.16	244.8	-48.7	342.4	-34.2	35.8	13.0
17	97-102	6	6	E 80° 42.674	N 47° 31.13	254.7	-39.6	328.8	-24.7	149.8	5.5
18	103-108	5	6	E 80° 41.402	N 47° 31.06	249.9	-19.6	335.9	-13.2	55.8	10.3
19	109-114	5	6	E 80° 41.423	N 47° 31.09	244.2	-35.0	340.0	-23.2	275.9	4.6
20	115-120	1	6	E 80° 41.430	N 47° 31.10	-	-	-	-	-	-
21	121-126	2	6	E 80° 41.453	N 47° 31.09	-	-	-	-	-	-
22	127-130	4	4	E 80° 40.782	N 47° 30.39	259.2	-48.8	323.1	-32.3	45.8	13.7
23	131-134	1	4	E 80° 40.763	N 47° 30.39	-	-	-	-	-	-
24	135-138	4	4	E 80° 40.624	N 47° 30.39	271.5	-31.5	312.5	-18.6	6.4	39.5
25	139-142	2	4	E 80° 40.580	N 47° 30.43	-	-	-	-	-	-
26	143-146	3	4	E 80° 40.570	N 47° 30.44	-	-	-	-	-	-
27	147-150	3	4	E 80° 40.524	N 47° 30.45	245.5	-38.3	338.3	-25.3	13.2	35.3
28	151-154	0	4	E 80° 40.395	N 47° 30.46	-	-	-	-	-	-
29	155-158	0	4	E 80° 40.395	N 47° 30.46	-	-	-	-	-	-
30	159-162	0	4	E 80° 40.281	N 47° 30.49	-	-	-	-	-	-

<u>Site</u>	<u>Sample Range</u>	<u>N1</u>	<u>N2</u>	<u>GPS Long.</u>	<u>GPS Lat.</u>	<u>Dg</u>	<u>Ig</u>	<u>VGP Long.</u>	<u>VGP Lat.</u>	<u>k</u>	<u>Q₉₅</u>
31	163-166	3	4	E 80° 40.303	N 47° 30.49	235.2	-45.7	348.1	-32.6	31.6	22.3
32	167-170	4	4	E 80° 43.621	N 47° 31.47	241.3	-38.1	339.9	-26.8	6.2	40.2
33	171-174	1	4	E 80° 43.654	N 47° 31.47	-	-	-	-	-	-
34	175-178	4	4	E 80° 43.687	N 47° 31.48	248.4	-22.4	337.0	-14.9	59.2	12.0
35	179-182	2	4	E 80° 43.734	N 47° 31.52	-	-	-	-	-	-
36	183-186	2	4	E 80° 43.784	N 47° 31.52	-	-	-	-	-	-
37	187-190	1	4	E 80° 43.873	N 47° 31.51	-	-	-	-	-	-
38	191-194	4	4	E 80° 43.910	N 47° 31.50	259.8	-37.5	322.8	-22.8	21.1	20.5
39	195-198	3	4	E 80° 43.948	N 47° 31.49	253.8	-51.2	237.1	-34.2	19.4	28.3
40	199-202	3	4	E 80° 43.978	N 47° 31.49	259.8	-25.6	325.3	-14.9	635.2	4.9
41	203-206	4	4	E 80° 43.995	N 47° 31.49	244.2	-17.7	341.5	-13.0	54.2	12.6
42	207-210	3	4	E 80° 44.034	N 47° 31.50	260.1	-26.2	325.1	-15.2	121.1	11.3
43	210-215	0	4	E 80° 44.257	N 47° 31.40	-	-	-	-	-	-
44	215-218	3	4	E 80° 44.226	N 47° 31.40	272.1	-19.9	313.7	-9.8	151.5	10.1
45	219-222	4	4	E 80° 44.168	N 47° 31.41	243.1	-33.5	341.3	-22.6	61.2	11.8
46	223-226	3	4	E 80° 44.145	N 47° 31.42	256.9	-20.8	328.4	-12.9	40.3	19.7
47	227-230	1	4	E 80° 44.099	N 47° 31.43	-	-	-	-	-	-
48	231-234	4	4	E 80° 42.269	N 47° 31.21	254.4	-41	330.2	-26.5	14.6	24.9
49	235-238	3	4	E 80° 43.205	N 47° 31.34	-	-	-	-	-	-
50	239-242	3	4	E 80° 43.172	N 47° 31.32	-	-	-	-	-	-
51	243-246	4	4	E 80° 43.116	N 47° 31.33	253.0	27.5	332.2	-17.2	55.8	12.4
52	247-250	4	4	E 80° 43.089	N 47° 31.30	246.6	-38.7	337.0	-25.6	120.1	11.3
53	251-254	4	4	E 80° 43.084	N 47° 31.26	268.2	-27.9	317.3	-15.5	39.4	14.8
54	255-258	4	4	E 80° 43.004	N 47° 31.19	271.2	-33.3	313.2	-17.9	139.2	7.8
55	259-262	4	4	E 80° 43.013	N 47° 31.16	245.1	-35.7	339.0	-23.4	180.5	6.9
56	263-266	4	4	E 80° 43.999	N 47° 31.12	234.6	-27.9	349.9	-20.2	18.2	22.1
57	267-270	4	4	E 80° 42.935	N 47° 31.06	254.2	-43.2	328.8	-27.3	123.3	8.3
58	271-274	4	4	E 80° 42.883	N 47° 31.05	249.4	-43.9	334.4	-29.1	23.8	25.9
59	275-278	4	4	E 80° 42.634	N 47° 31.15	264.9	-40.6	318.6	-24.4	24.9	18.8
60	279-282	3	4	E 80° 42.625	N 47° 31.14	259.4	-45.8	323.1	-28.7	245.3	7.9

Table 2: Site information yielded from tilt corrected site data.

<u>Site</u>	<u>Sample Range</u>	<u>N1</u>	<u>N2</u>	<u>GPS Long.</u>	<u>GPS Lat.</u>	<u>Ds</u>	<u>Is</u>	<u>VGP Long.</u>	<u>VGP Lat.</u>	<u>k</u>	<u>Q95</u>
1	1-6	5	6	E 80° 42.205	N 47° 31.27	272.5	-47.4	308.7	-27.9	12.2	22.8
2	7-12	4	6	E 80° 42.140	N 47° 31.27	227.6	-58.3	352.5	-45.2	16.4	19.5
3	13-18	6	6	E 80° 42.138	N 47° 31.36	229.4	-46.4	352.5	-34.2	35.6	11.4
4	19-24	6	6	E 80° 42.147	N 47° 31.47	236.5	-54.8	344.4	-40.4	76.5	7.7
5	25-30	6	6	E 80° 42.139	N 47° 31.57	256.7	-45.8	327.4	-29.9	11.7	23.3
6	31-36	6	6	E 80° 42.155	N 47° 31.59	255.0	-59.9	325.1	-43.5	39.5	10.8
7	37-42	5	6	E 80° 41.890	N 47° 31.19	244.1	-63.0	333.6	-48.4	39.9	12.3
8	43-48	5	6	E 80° 41.877	N 47° 31.15	250.7	-62.0	328.7	-45.7	12.9	22.2
9	49-54	5	6	E 80° 41.871	N 47° 31.17	281.1	-42.4	302.3	-22.8	27.5	14.9
10	55-60	3	6	E 80° 41.86	N 47° 31.19	219.3	-58.4	2.6	-48.0	19.6	28.6
11	61-66	4	6	E 80° 41.871	N 47° 31.23	247.9	-61.0	330.4	-45.0	12.6	22.4
12	67-72	5	6	E 80° 41.652	N 47° 31.15	218.8	-39.5	6.5	-30.4	18.6	18.2
13	73-78	6	6	E 80° 41.826	N 47° 31.14	253.1	-57.7	326.3	-41.3	14.7	18.1
14	79-84	5	6	E 80° 41.749	N 47° 31.15	251.9	-58.3	327.8	-41.7	46.1	11.4
15	85-90	6	6	E 80° 41.781	N 47° 31.16	250.3	-60.1	329.0	-43.6	28.4	12.8
16	91-96	6	6	E 80° 41.814	N 47° 31.16	230.5	-65.8	346.7	-53.7	22.4	16.5
17	97-102	6	6	E 80° 42.674	N 47° 31.13	255.0	-57.6	324.9	-40.1	96.8	6.8
18	103-108	5	6	E 80° 41.402	N 47° 31.06	249.1	-37.6	334.9	-24.1	43.3	11.8
19	109-114	5	6	E 80° 41.423	N 47° 31.09	240.7	-52.7	340.8	-37.6	161.2	6.0
20	115-120	1	6	E 80° 41.430	N 47° 31.10	-	-	-	-	-	-
21	121-126	2	6	E 80° 41.453	N 47° 31.09	-	-	-	-	-	-
22	127-130	4	4	E 80° 40.782	N 47° 30.39	262.6	-66.7	313.8	-51.7	21.4	20.3
23	131-134	1	4	E 80° 40.763	N 47° 30.39	-	-	-	-	-	-
24	135-138	4	4	E 80° 40.624	N 47° 30.39	276.7	-48.4	302.0	-32.5	4.8	47.2
25	139-142	2	4	E 80° 40.580	N 47° 30.43	-	-	-	-	-	-
26	143-146	1	4	E 80° 40.570	N 47° 30.44	-	-	-	-	-	-
27	147-150	3	4	E 80° 40.524	N 47° 30.45	242.0	-56.0	338.3	-40.9	9.5	42.5
28	151-154	0	4	E 80° 40.395	N 47° 30.46	-	-	-	-	-	-
29	155-158	0	4	E 80° 40.395	N 47° 30.46	-	-	-	-	-	-
30	159-162	0	4	E 80° 40.281	N 47° 30.49	-	-	-	-	-	-

<u>Site</u>	<u>Sample Range</u>	<u>N1</u>	<u>N2</u>	<u>GPS Long.</u>	<u>GPS Lat.</u>	<u>Ds</u>	<u>Is</u>	<u>VGP Long.</u>	<u>VGP Lat.</u>	<u>k</u>	<u>Q95</u>
31	163-166	3	4	E 80° 40.303	N 47° 30.49	225.1	-62.2	355.4	-50.3	18.8	29.3
32	167-170	4	4	E 80° 43.621	N 47° 31.47	236.2	-55.5	340.6	-42.8	4.3	50.7
33	171-174	1	4	E 80° 43.654	N 47° 31.47	-	-	-	-	-	-
34	175-178	4	4	E 80° 43.687	N 47° 31.48	247.2	-40.3	336.1	-26.3	47.2	13.5
35	179-182	2	4	E 80° 43.734	N 47° 31.52	-	-	-	-	-	-
36	183-186	2	4	E 80° 43.784	N 47° 31.52	-	-	-	-	-	-
37	187-190	1	4	E 80° 43.873	N 47° 31.51	-	-	-	-	-	-
38	191-194	4	4	E 80° 43.910	N 47° 31.50	262.2	-55.4	316.4	-37.3	12.8	26.7
39	195-198	3	4	E 80° 43.948	N 47° 31.49	253.6	-69.2	319.7	-54.7	11.9	37.4
40	199-202	3	4	E 80° 43.978	N 47° 31.49	261.3	-43.5	321.7	-26.4	449.7	5.8
41	203-206	4	4	E 80° 43.995	N 47° 31.49	242.5	-35.4	341.3	-23.7	43.6	14.1
42	207-210	3	4	E 80° 44.034	N 47° 31.50	261.6	-44.1	321.4	-26.8	91.0	13.0
43	210-215	0	4	E 80° 44.257	N 47° 31.40	-	-	-	-	-	-
44	215-218	3	4	E 80° 44.226	N 47° 31.40	275.4	-36.8	308.6	19.5	104.7	12.1
45	219-222	4	4	E 80° 44.168	N 47° 31.41	239.5	-51.1	342.5	-36.7	40.0	14.7
46	223-226	3	4	E 80° 44.145	N 47° 31.42	257.5	-38.7	325.5	-24.1	28.3	23.6
47	227-230	1	4	E 80° 44.099	N 47° 31.43	-	-	-	-	-	-
48	231-234	4	4	E 80° 42.269	N 47° 31.21	254.6	-59.0	327.1	-43.1	9.2	32.1
49	235-238	2	4	E 80° 43.205	N 47° 31.34	-	-	-	-	-	-
50	239-242	3	4	E 80° 43.172	N 47° 31.32	251.8	-41.3	327.7	-26.7	4.4	67.5
51	243-246	4	4	E 80° 43.116	N 47° 31.33	252.7	-45.5	330.5	-29.6	41.2	14.5
52	247-250	4	4	E 80° 43.089	N 47° 31.30	243.5	-56.5	336.8	-41.4	62.4	15.7
53	251-254	4	4	E 80° 43.084	N 47° 31.26	271.9	-45.2	311.8	-27.4	27.9	17.7
54	255-258	4	4	E 80° 43.004	N 47° 31.19	276.7	-50.6	305.1	-29.8	80.4	10.3
55	259-262	4	4	E 80° 43.013	N 47° 31.16	241.8	-53.4	339.6	-38.0	120.5	8.4
56	263-266	4	4	E 80° 43.999	N 47° 31.12	229.6	-44.7	352.3	-32.6	15.7	23.9
57	267-270	4	4	E 80° 42.935	N 47° 31.06	254.4	-61.2	324.6	-44.1	81.2	10.3
58	271-274	3	4	E 80° 42.883	N 47° 31.05	246.9	-61.9	333.2	-46.7	14.7	33.4
59	275-278	4	4	E 80° 42.634	N 47° 31.15	269.8	-58.2	310.3	-39.7	15.4	24.2
60	279-282	3	4	E 80° 42.625	N 47° 31.14	262.5	-63.7	315.2	-46.1	106.0	12.0

9. References:

- Abrajevitch, A., Van der Voo, R., Bazhenov, M. L., Levashova, N. M., and McCausland, P. J. A., 2008, The role of the Kazakhstan orocline in the late Paleozoic amalgamation of Eurasia, *Tectonophysics*, 2008, v. 455, 61–76.
- Alexeiev, Dmitriy, and Kirill Degtyarev. "Accretionary tectonics of Kazakhstan: Main features and principles of reconstruction." *International Geological Congress OSLO 2008*. International Geological Congress, n.d. Web. 7 Mar 2013.
<<http://www.cprm.gov.br/33IGC/1203760.html>>.
- Bazhenov, M., Van der Voo, R., Levashova, N., & Dominguez, A. (2013). Late devonian palaeomagnetism of the north tien shan, kyrgyzstan: can secular variation vary on a short timescale?. *Geophysical Journal International*, Retrieved from
<http://gji.oxfordjournals.org/content/early/2013/02/14/gji.ggt011.short>
- Biggin, A. J., Strik, G. H. M. A., and Langereis, C. G., 2008. Evidence for a very-long-term trend in geomagnetic secular variation, *Nature Geosci.*, v. 1, 395-398.
- Biggin, A. (2012). Section b2: The scientific proposal inferring mantle dynamics from geomagnetic evolution. In *IMAGE*.
- Butler, Robert. *PALEOMAGNETISM Magnetic Domains to Geologic Terranes*. Blackwell Scientific Publications, 1992. eBook. <<http://faculty.up.edu/butler/books/main.htm>>.
- Dominguez, Ada. "On the Behavior of the Geomagnetic Field During the Miocene." . University of Michigan, 24 2012. Web. 7 Mar 2013.
- Dunlop, David. "On the use of Zijderveld vector diagrams in multicomponent paleomagnetic studies." *Elsevier*. 20.1 (1979): 12-24. Web. 31 Mar. 2013.
<<http://www.sciencedirect.com/science/article/pii/0031920179901031>>.
- Heunemann, C., R. Leonhardt, and D. Krasa. "Analyzing absolute paleointensity determinations: Acceptance criteria." *Geochemistry, Geophysics, Geosystems*. 5.12 (2004): n. page. Web. 5 Apr. 2013.

<<http://onlinelibrary.wiley.com.proxy.lib.umich.edu/doi/10.1029/2004GC000807/abstract;jsessionid=8B483D3D7DB6A7266B753A87AE72B97B.d04t04>>.

- Levashova, N. M., Degtyarev, K.E., Bazhenov, M. L., Collins, A. Q., and Van der Voo, R., 2003a. Permian Paleomagnetism of East Kazakhstan and the amalgamation of Eurasia, *Geophys. J. Intern.*, v. 152, 677-687.
- Levashova, N. M., Mikolaichuk, A. V., McCausland, P. J. A., Bazhenov, M. L., and Van der Voo, R., 2007. Devonian paleomagnetism of the North Tian Shan: implications for the middle-late Paleozoic paleogeography of Eurasia, *Earth Planet. Sci. Lett.*, v. 257, 104 – 120.
- McFadden, P.L, Merrill, R.T., McElhinny, M.W., and Lee, S., 1991. Reversals of the Earth's magnetic field and temporal variations of the dynamo families, *J. Geophys. Res.*, v. 96, 3923-3933.
- Sal'menova, K.Z. & Koshkin, V.Y., 1990. *Stratigraphy and Flora of the Late Paleozoic in the North Balkhash Area*, p. 160, Almaty, Navka.
- Tarduno, J.A., Cottrell, R. D., and Smirnov, A. V., 2002. The Cretaceous superchron geodynamo: Observations near the tangent cylinder, *PNAS*, v. 99, 14020–14025.
- Tauxe, L., Hartl, P., 1997. 11 million years of Oligocene geomagnetic field behaviour. *Geophysical Journal International* 128, 217– 229.
- Tauxe, L. and D.V. Kent, 2004, A simplified statistical model for the geomagnetic field and the detection of shallow bias in paleomagnetic inclinations: Was the ancient magnetic field dipolar? in J.E.T. Channell, D.V. Kent, W. Lowrie and J. Meert (editors), *Timescales of the Paleomagnetic Field*, AGU Geophysical Monograph 145, 101-115.
- Van der Voo, R., Levashova, N.M., Skrinnik, L.S., Kara, T.V., and Bazhenov, M.L., 2006. Late orogenic, large-scale rotations in the Tien Shan and adjacent mobile belts in Kyrgyzstan and Kazakhstan, *Tectonophysics*, v. 426, 335-360.